20th Australasian Fluid Mechanics Conference
Perth, Australia
5-8 December 2016

A numerical investigation of the human-induced wake during gait cycles in the indoor environment

Yao Tao[1], Kiao Inthavong[1] and Jiyuan Tu[1]
1 School of Engineering,
RMIT University, Bundoora, Victoria, 3083, Australia

Abstract

The characteristics of human-induced wake in an indoor environment was investigated by performing CFD simulations of a manikin in a confined room. The manikin motion with and without limbs' swinging were achieved by the dynamic mesh method to update the new grids with each time step. The spatial and temporal characters of wake flow induced by the two motion modes was compared. Results indicated the common features of the wake flow at different part of the body, such as the significant downwash at the back and the upwash through the gap of legs. By comparing the flow field generated by rigid motion and swinging motion, significant discrepancies were found in terms of the velocity field and the vorticity distribution, especially at the lower part of the body which could be influential on the contaminant dispersion. The swinging limbs increased the airflow disturbances around the limbs and also influenced the region behind the torsos comparing to the rigid motion.

Introduction

The human activity has been identified to wield significant influence on indoor airflow patterns by producing distinct wake flow regions and unsteady vortex shedding over the body [1-3]. Its consequences on the indoor contaminant transport and dispersion [4-6] received lots of attention especially in interior environments such as aircraft cabins, hospital wards, surgical rooms and cleanrooms, where occupants' exposure levels to airborne contaminants are highly valued [7-9].

The human-induced wake flow showed similarities with the boundary layer separation when air flowed over bluff bodies, forming a mixing zone that vortices entraining air into a reverse flow region [10]. A number of studies had provided insights into main aerodynamic features of flow over finite vertical cylinders [11], such as the tip vortices around the free end, horseshoe vortex at the bottom, arch vortex attached to the ground, and recirculation region extending downstream behind the body. Therefore, simplified geometries such as cuboids were used as substitutes of human bodies at earlier stages [12,13]. However, discrepancies in flow features due to geometry differences were also found, i.e. the legs could be considered as two closely arranged cylinders whose wake flow interacted with each other depending on the gap width [10]. On the other hand, many studies considered the body as stationary in a domain with a constant incoming flow. With simplified geometries and stationary assumptions, the dynamic effects of wind on human bodies had identified wake regions and unsteady vortex shedding, by experimental and numerical studies [1,2] However, the assumption of relative motion between the flow and the stationary body neglected the flow disturbance caused by the manikin motion, hence partially represented the near wake characteristics of human wake during walking.

Recently more studies emphasized on the effects of realistic human motion in the indoor environments, and used anthropomorphic manikins than simplified geometries since they provided more accurate results on the near-body regions [14]. Han, Weng, Huang, Fu, Yang and Luo [15] experimentally measured the motion-induced flow fields around a full-scale manikin under rigid motion and stationary swinging. They found the characteristics of wake flow related to pendulum frequency, walking speeds and the spatial location. Numerically, by applying dynamic mesh methods in the CFD approach, some studies had obtained the visualization of human induced wake region. Hang et al (2014) investigated the influences of human walking on the indoor airflow and airborne transmission, and found the walking indeed enhanced the airborne transmission from the source manikin though its influence was minor compared to the ventilation. Choi and Edwards [16] studied the human-induced contaminant transport in room compartments with a moving human model achieved by a human kinematics model, and found that the transport mechanism of particle consisted of the entrainment into the human induced wake and the backward transport due to downwash effect and tip vortex formation.

Moreover, buoyancy-driven flow from body surfaces was influential on the airflow patterns around the human body. The thermal plume near the body could be comparable with the wake flow under a low moving speed, but when the moving speed was larger than 0.4 m/s, the wake flow re-dominates the micro-environment airflow patterns near the moving body [17]. Due to the complex shape of human, some detailed information such as the air flow field in the close vicinity of a person and convective heat transfer between human body and surroundings can hardly be obtained by experiments [14]. Comparing to experimental studies, Computational Fluid Dynamics (CFD) approaches have become more popular in studying indoor air flows [18] and human wake [16], owing to advantages of low-cost and powerful visualization capabilities. CFD methods with dynamic mesh technique have been validated able to qualitatively capture the fundamental flow features of the wake flow characteristics induced by obstacle motion [12]

The studies into human-induced wake flow are gradually developing its accuracy and integrating with air quality assessment. However, some characteristics of the dynamic wake induced by walking process remains unclear. Very few researches compared the discrepancies induced by different motion modes used by previous research, i.e. the rigid motion (no limbs swinging) and the swinging motion (in gait cycles), to indicate the differences that might arise in evaluating the dynamic flow field. Along with the lack of focuses on the residual wake flow patterns when the human body came to stop, which could be equally important if contaminants were not removed instantly from the confined space.

In the present study, numerical methods were adopted to investigate the details of wake flow induced by a thermal manikin in the indoor environment under two motion modes, focusing on the discrepancies in the flow field and vortex structures induced by motion with and without limbs swinging during and after the manikin's moving. Techniques related to dynamic mesh modelling was applied in the simulation to achieve the motion. It is expected

to improve the further assessment on contaminants levels for indoor air quality based on more accurate prediction of human-induced wake.

Numerical methods

Cylinder Geometry for Model Validation

The fluid dynamics of wake flow around human body conforms to the fundamental behaviour of boundary layer separation of flows over bluff bodies [2]. To validate the numerical modelling accuracy, simulations of near wake flow around vertical cylinders were conducted and validated against PIV measurements by Rostamy, Sumner, Bergstrom and Bugg [19]. The computational domain was a cuboid with dimensions of 1.96m × 0.91m × 1.13m. A circular cylinder with a diameter of 31.5mm and an aspect ratio (H/D) of 3 was fixed on the ground. The vertical cylinder has similar aspect ratio with our manikin model (discussed later). The free stream velocity was U = 20 m/s, turbulence intensity less than 0.6%, giving a Reynolds number of 42000 based on the cylinder diameter.

To solve the boundary layer separation in the viscous sub-layer on the cylinder surface, 10 prism cell layers were extruded from the surface with an initial grid spacing of 1×10^{-4} m. This produced a dimensionless wall distance (y+) of less than 5 to keep the first grid point within the viscous sub-layer, and ensured a sufficient number of grid points within the buffer region where turbulent production rapidly increases. A structured hexahedral mesh with a total 3.1 million cells was generated. The flow domain was calculated by applying ambient flow conditions with the experiment data, and the time step size for the transient flow was 1×10^{-3} s.

Indoor Room Model Geometry and Boundary conditions

A manikin with a height of 1.7m was initially standing in a 4.6m ×6m×2.7 m quiescent room, with a distance of 1 meter to the back wall as shown in Figure 1(a). The manikin was assigned to a fixed surface temperature of 34℃, with the air temperature given as 24℃. Unstructured tetrahedral cells and prism layers were generated around the manikin surface (Figure 1(b)). To capture boundary layer separation around the manikin, 10 prism layers were generated on the manikin surface to keep the dimensionless wall distance y+ < 5.

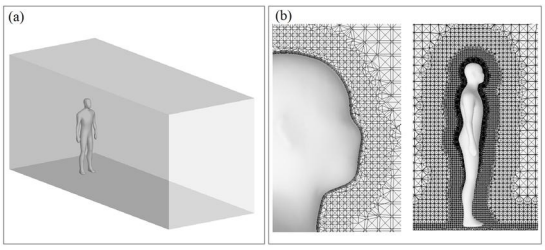

Figure1 (a) Computational domain of the room; (b) Prism layers and mesh generation around the manikin.

The cadence (the number of steps per unit time) and the walking speed of a person are subject to various factors. We assumed a medium walking speed that 2 steps finished in one second with a mean walking speed of 1.2 m/s according to the findings from [20]. In order to reduce the calculation of dynamic meshes, the walking gestures were simplified as no bending of knees and elbows, only swung as pendulums starting from the root of big arms and thighs. Maximum joint angle displacements for arms and elbows are 15°and 30° respectively. The gait cycle was achieved by defining the rotating velocities of limbs during each gait phase using UDF in commercial CFD software ANSYS Fluent. The rotating velocities were calculated from the length of limbs, the gait period (1s) and the walking speed (1.2m/s).

Flow and heat transfer models

For a three-dimensional time-dependent turbulent and buoyant flow of an incompressible fluid, the Reynolds-average Navier-Stokes equations (RANS) are solved for the fluid phase. The general transport equation where continuity, momentum equations, turbulent quantities and energy are given is stated as equation (1):

$$\frac{\partial(\rho\phi)}{\partial t}+\frac{\partial(\rho u_i\phi)}{\partial x_i}=\frac{\partial}{\partial x_i}\left(\Gamma\frac{\partial\phi}{\partial x_i}\right)+S_\phi \qquad (1)$$

where, Φ represents the general variables, Γ represents the diffusion coefficient and S_Φ represents the source term, u_i is the velocity component in i direction, the expressions for Φ and S corresponded to each transported variable. In the thermal condition, the buoyant forces resulted from the density gradients in the vertical direction was calculated by Boussinesq approximation. The human motion was achieved by integrating dynamic mesh technique. Re-meshing method was adopted to update the deformed meshes before every time step in the unsteady process. Model validation compared the RNG k-ε model with the Shear Stress Transport (SST) turbulence model. The discretization involved the QUICK scheme for momentum, and the SIMPLE algorithm for pressure-velocity coupling. The second-order upwind scheme was used for the convection and diffusion terms. A time step which of 0.005s and the mesh was updated at each time step matching the manikin movement.

Results

Air flow patterns across a vertical cylinder

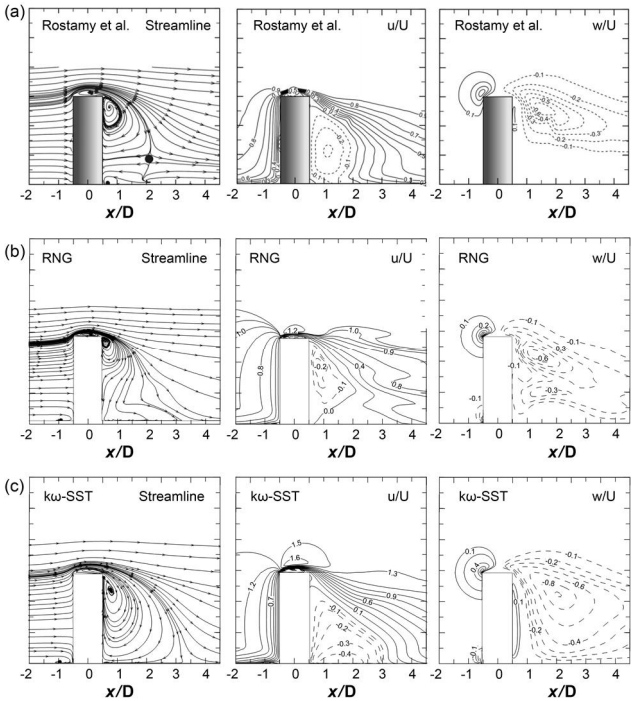

Figure 2. Comparisons of streamlines, normalized u-velocity component (u/U), normalized w-velocity component (w/U) on the mid-plane between (a) PIV measurement data; (b) CFD results using RNG turbulence model; (c) CFD results using kω-SST turbulence model.

The averaged velocity field on the centre plane of flow across a vertical cylinder were compared with the measured data by Rostamy, Sumner, Bergstrom and Bugg [19] (Figure 2). The immediate downstream flow that originated around the free end (top cylinder surface, free from other surfaces), and persisting in the stream-wise direction was observed from in the simulated results. The stream-wise counter-rotating vortex within the wake were captured, one was the tip vortex near the free end and the other was the base vortices near the cylinder-wall junction. Minor

differences occurred at the locations of the saddle points related to the two vortices, and the prediction in the u and w velocity components. The RNG model showed better performance over the kw-SST in predicting the velocity distribution in the near wake region. Overall, the reasonably good agreement from the comparisons showed that the proposed numerical approach was reliable for wake flow prediction behind a bluff-body.

Airflow field under rigid and swinging body motion

The comparisons between the rigid motion and the swinging motion under thermal conditions are made in Figure 3 in terms of the instantaneous velocity variation against time. Three sets of points moving with the manikin were set at 20 mm to the limb surfaces on the inner side (near-torso) and the farther side of the arm, the thigh and the ankle respectively. Starting from 0 sec, the swinging right arm and left leg were preparing to move forward relative to the torso while the other limbs were moving oppositely.

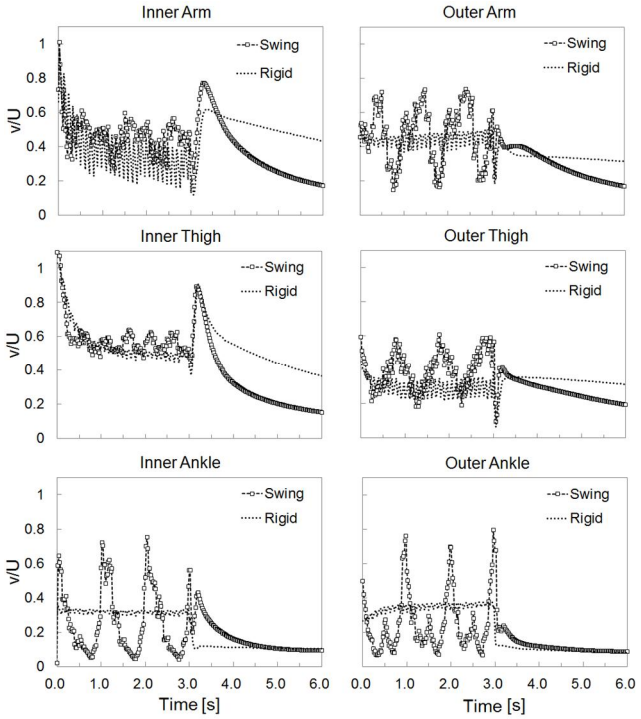

Figure 3 Velocity comparisons of rigid motion and swinging motion at 3 sets of points (inner and outer side of arm, thigh and leg) against time

In the rigid motion, obvious oscillating flow induced by the vortex shedding was captured, showing as limited amplitudes of instantaneous velocity distribution occurred with a frequency. The phenomenon is similar to the characters of vortex shedding produced by bluff bodies that interacted with an external fluid flow and produced periodical irregularities on the flow characters. When vortices were formed at the back region of the body and detached periodically from one side to the other, unsymmetrical lift forces perpendicular to the inflow developed on each side, thus leading to motion transverse to the flow. Regarding the arm, the thigh and the ankle as cylinders with diameters of 0.1m, 0.2m and 0.08m, their corresponding Reynolds numbers of 9,000, 16,000, 6,400 were in the sub-critical Reynolds numbers range, in which the shedding tends to be organized with an almost constant non-dimensional vortex shedding frequency according to external flow over a cylinder.

However, in the swinging motion, velocity magnitudes and directions were re-dominated by the swinging momentum, showing as periodic peaks and dips corresponding to full gait cycles, while the amplitudes of vortex oscillation became minor. The velocities collected at the detection points varied with the relative motion of limbs to the points. Taking the left ankle for example, velocities at the points were decreasing when the ankle were moving away from the point, while increasing when it moved towards the point by pushing the air in the swinging direction, and drawn the air around to entrain the wake.

Velocity discrepancies between the two motion modes majorly occurred during the walking process, more distinct at the lower part of the body. The inner points around arms and thighs were less influenced due to the confinement from body structures thus showing similar characters under the two motion modes. Since the farther side and the region around the ankle had less limited space for wake flow to develop, the motion at those areas induced by swinging showed a different pattern. A larger velocity amplitude induced by swinging occurred at the lower body such as the ankle. The highest velocities induced by the swinging leg would generate 2 times of the velocity under the rigid motion at the ankle's height during walking, which would yield considerable influence on floor-board contaminants dispersion.

When the manikin came to stopped at t = 3s, the residual momentum had led to notable velocity rises especially at the near-body region. The residual wake flow propagated from the rear to the front of the manikin through the narrow gaps between the limb and the torso, hence generating an immediate velocity rise after its stop. The swinging motion had experienced a larger increase in velocities at those areas due to the inertia yielded by the swinging of limbs. While at the points around the arm and the thigh, the wake tailed away much quicker in the swinging motion than in the rigid motion. It showed the use of rigid motion might over-predict the influence on the wake around the upper body when the motion stopped.

Flow Field Characters

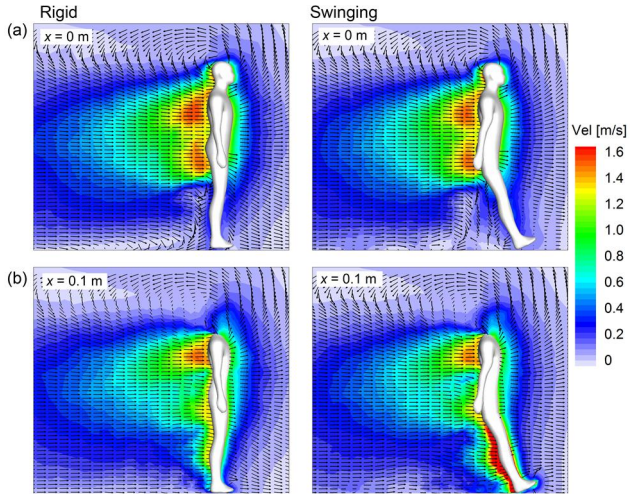

Figure 4 Velocity contours and vectors on (a) mid-plane x = 0.0 m (mid-plane) (b) plane x = 0.12 m (through the leg) at t = 2.75s

Figure 4 showed the velocity contours and vectors on the mid-plane (X = 0m) and the plane through the right leg (X = 0.12 m) under two motion modes at t = 2.75 s, when the limbs were stretching in the final cycle before its stop. At the upper body, the shed airflow formed downwash flow towards the back where the highest velocities were observed. The flow patterns showed similarities under two motion modes, however the rigid motion predicted a larger region of high velocities. Noticeable discrepancies were found at the lower region behind the gap of legs, which showed a significant air movement induced by the swinging motion, while the rigid motion predicted a calmer and shorter area in terms of flow disturbances.

Figure 5 showed the contour of vorticity magnitude ω_x, ω_y, ω_z in the mid-plane across the body (X = 0 m), the vertical plane 0.2 m

behind the manikin (Y = 3.4 m) and the horizontal plane through the waist (Z = 1.1 m) at t = 2.75s. In the mid-plane, a strong negative vorticity concentration convected from the head and shoulders, indicating an anti-clockwise circulation region at the back of the upper body where the significant downwash occurred. Besides, a strong positive vorticity protruding from the gap of the legs identified a clock-wise circulation against the downwash circulation behind the upper body. Re-circulations regions were formed behind the solid torso during manikin's walking.

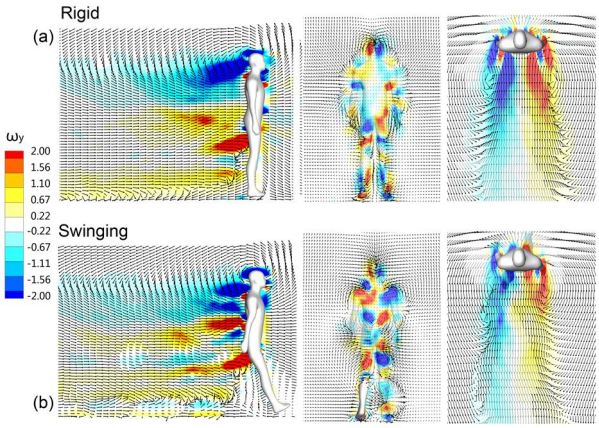

Figure 5 instantaneous vorticity field under rigid motion and swinging motion at plane X = 0 m, Y = 3.4m, Z = 1.1 m

In the swinging motion, several pairs of counter-rotating vortices were generated behind the head, the torso and legs, on the vertical plane behind the body. While in the rigid body motion, smaller region and lower strength of vorticities was observed in the same area. The asymmetric vortex shedding in the horizontal plane interacted with the downwash and up-wash flows, thus inducing the laterally and vertically spread from the upper body towards the downstream region. The counter-rotating vortex shedding then stretched downwards into the wake region. Downstream the walking body, the vortices diffused away quicker than the rigid motion showing as the subdued span-wise vortex shedding and the lower vorticity concentration on the horizontal plane, as a result of stronger interactions from the counter-rotating circulations behind the swinging motion with the stream-wise vorticities.

Conclusions

This paper discussed the human-induced wake flow in the indoor environment simulated under two motion modes: the rigid motion with no limbs swinging and the swinging motion according to human gait cycle. Although the swinging motion and the rigid body motion yielded wake regions with similar characters, the velocity and vorticity distribution during walking showed discrepancies, especially at the lower part of the body. The maximum velocity at the ankle could be roughly twice as large as that rigid body yielded. The motion with limbs swinging produced more disturbances along the walking path, especially behind the gap of legs that observed a longer region of stronger air movement rather than the stagnant region under the rigid motion. The discrepancies might exert important influence the contaminant transport from the ground. In the future studies of indoor contaminant dispersion, the swinging of limbs showed its significance to improving the accuracy of evaluation for indoor exposure levels.

Acknowledgments

The authors would like to acknowledge the financial support provided by the Australian Research Council (Project ID: DP160101953), and the resources provided at the NCI National Facility Systems at the Australian National University through the National Computational Merit Allocation Scheme supported by the Australian Government.

References

[1] Murakami S, Zeng J, and Hayashi T, CFD analysis of wind environment around a human body. *Journal of Wind Engineering and Industrial Aerodynamics* 1999; 83(1–3): 393-408.

[2] Edge BA, Paterson EG, and Settles GS, Computational Study of the Wake and Contaminant Transport of a Walking Human. *Journal of Fluids Engineering* 2005; 127(5): 967-977.

[3] Ge Q, Li X, Inthavong K, and Tu J, Numerical study of the effects of human body heat on particle transport and inhalation in indoor environment. *Building and Environment* 2013; 59(0): 1-9.

[4] Mazumdar S, Poussou SB, Lin C-H, Isukapalli SS, Plesniak MW, and Chen Q, Impact of scaling and body movement on contaminant transport in airliner cabins. *Atmospheric Environment* 2011; 45(33): 6019-6028.

[5] Miguel AF, Aydin M, and Reis AH, Indoor Deposition and Forced Re-suspension of Respirable Particles. *Indoor and Built Environment* 2005; 14(5): 391-396.

[6] Inthavong K, Ge QJ, Li XD, and Tu JY, Detailed predictions of particle aspiration affected by respiratory inhalation and airflow. *Atmospheric Environment* 2012; 62(0): 107-117.

[7] Inthavong K, Ge QJ, Li A, and Tu JY, Source and trajectories of inhaled particles from a surrounding environment and its deposition in the respiratory airway. *Inhalation Toxicology* 2013; 25(5): 280-291.

[8] Li X, Inthavong K, and Tu J, Numerical investigation of micron particle inhalation by standing thermal manikins in horizontal airflows. *Indoor and Built Environment* 2014.

[9] Se CMK, Inthavong K, and Tu J, Inhalability of micron particles through the nose and mouth. *Inhalation Toxicology* 2010; 22(4): 287-300.

[10] Flynn MR and Ljungqvist B, A REVIEW OF WAKE EFFECTS ON WORKER EXPOSURE. *Annals of Occupational Hygiene* 1995; 39(2): 211-221.

[11] WANG HF and ZHOU Y, The finite-length square cylinder near wake. *Journal of Fluid Mechanics* 2009; 638: 453-490.

[12] Poussou SB, Mazumdar S, Plesniak MW, Sojka PE, and Chen Q, Flow and contaminant transport in an airliner cabin induced by a moving body: Model experiments and CFD predictions. *Atmospheric Environment* 2010; 44(24): 2830-2839.

[13] Thatcher TL, Wilson DJ, Wood EE, Craig MJ, and Sextro RG, Pollutant dispersion in a large indoor space: Part 1 – Scaled experiments using a water-filled model with occupants and furniture. *Indoor Air* 2004; 14(4): 258-271.

[14] Gao NP and Niu JL, CFD Study of the Thermal Environment around a Human Body: A Review. *Indoor and Built Environment* 2005; 14(1): 5-16.

[15] Han ZY, Weng WG, Huang QY, Fu M, Yang J, and Luo N, Aerodynamic characteristics of human movement behaviours in full-scale environment: Comparison of limbs pendulum and body motion. *Indoor and Built Environment* 2015; 24(1): 87-100.

[16] Choi JI and Edwards JR, Large-eddy simulation of human-induced contaminant transport in room compartments. *Indoor Air* 2012; 22(1): 77-87.

[17] Wu Y and Gao NP, The dynamics of the body motion induced wake flow and its effects on the contaminant dispersion. *Building and Environment* 2014; 82: 63-74.

[18] Heschl C, Inthavong K, Sanz W, and Tu J, Nonlinear eddy viscosity modeling and experimental study of jet spreading rates. *Indoor Air* 2014; 24(1): 93-102.

[19] Rostamy N, Sumner D, Bergstrom DJ, and Bugg JD, Local flow field of a surface-mounted finite circular cylinder. *Journal of Fluids and Structures* 2012; 34: 105-122.

[20] Al-Obaidi S, Wall JC, Al-Yaqoub A, and Al-Ghanim M, Basic gait parameters: a comparison of reference data for normal subjects 20 to 29 years of age from Kuwait and Scandinavia. *J Rehabil Res Dev* 2003; 40(4): 361-6.